Low-frequency dynamics of a Nd-doped glass laser

Björn Peters,[1] Jörg Hünkemeier,[1] Valery M. Baev,[1] and Yakov I. Khanin[1,2]

[1]*Institut für Laser-Physik, Universität Hamburg, Jungiusstrasse 9, 20355 Hamburg, Germany*
[2]*Institute of Applied Physics, Russian Academy of Science, 46 Uljanov Street, 603 600 Nizhny-Novgorod, Russia*
(Received 6 February 2001; published 18 July 2001)

We study a Nd-doped microchip glass laser that emits in two polarizations and in many longitudinal modes. Saturation of the inversion by standing waves causes spatial inhomogeneity of both the longitudinal and azimuthal distributions of the laser gain. These nonlinear inhomogeneities couple the modes and result in low-frequency oscillations (10–500 kHz) of the light flux in the individual laser modes. These oscillations are steadily driven by quantum noise and appear as 15% fluctuations of the power in each mode. In-phase fluctuations in the laser modes appear at the frequency of the main relaxation oscillation of the total laser power. Antiphase fluctuations appear at other frequencies in individual longitudinal and polarization laser modes only. The dominant frequency of these fluctuations is determined by the light power in the mode. Numerical simulations of rate equations, including Langevin forces, satisfactorily reproduce the experimental results. These phenomena must be taken into account when lasers are applied as stable coherent optical light sources, and also with sensitive absorption measurements in the laser cavity.

I. INTRODUCTION

Practical applications of multimode lasers are often hampered by complex spectral dynamics of the output. The ultimate sensitivity of intracavity absorption measurements, for instance, is restricted by dynamic processes occurring in these lasers [1]. Theoretical consideration of rate equations for multimode solid-state or dye lasers predicts that the stationary laser emission is stable [2,3]. However, the damping rate of weak oscillations near the stationary state of such multimode laser is usually small. Therefore, even a very weak driving force, such as quantum fluctuations, may result in large scale fluctuations of the modal emission [3,4].

Nonlinear coupling of laser modes significantly modifies the dynamical properties of the system. Fluctuations of laser modes may become very strong, as has been observed with dye lasers [5]. Nonlinear mode coupling responsible for the emission dynamics of cw dye lasers has been identified as four-wave mixing by stimulated Brillouin scattering and population pulsations [5–7]. When the coupling is strong, the stationary solution becomes unstable, and the laser shows chaotic [8] or even periodic [9] spectral dynamics with its effective number of emitting modes reduced. Other types of mode coupling may be responsible for the instability of laser spectral dynamics as well, e.g., intracavity second-harmonic generation [10] or excited-state absorption [11]. With appropriate parameters of these lasers, mode coupling may also improve emission stability [12,13].

In contrast to dye lasers, solid-state lasers show decay rates of the upper laser level much smaller than the decay rate of the light in the cavity. Therefore the inversion does not follow adiabatically the light power, and the transient laser dynamics shows relaxation oscillations. A laser design frequently used in practice is that of chip solid-state lasers, with mirrors directly coated on both facets of the laser crystal and that is pumped by diode lasers [14–17]. This construction is useful for the investigation of the emission dynamics since it is not very sensitive to mechanical instabilities and

only a few modes oscillate. In these lasers the gain medium fills the entire length of the cavity, and both linear polarizations are excited. Spatial inhomogeneity ("hole burning") of the gain in longitudinal [18,19] and azimuthal directions [20] provides strong mode coupling in these lasers. It results in antiphase cross-saturation dynamics of the transient modal emission featuring low-frequency relaxation oscillations. Measurements performed with short cavities that are partly filled with gain medium [21–24] show similar features.

The stationary emission of a laser with spatial inhomogeneity is stable. Therefore, laser dynamics in solid-state lasers was studied frequently in the transient regime [14,16]. Alternatively, these lasers were investigated by introducing sinusoidal modulation of the pump power. This modulation leads to the resonant excitation of relaxation oscillations and, if this modulation is strong, to period doubling, bifurcation, and to chaotic relaxation oscillations [15]. However, experiments show that the individual modes of these lasers are fluctuating even in the stationary state [15,17] predominantly at the frequencies of relaxation oscillations. It has been suggested that this is the result of technical noise and it has been modeled by introducing an auxiliary noise source in the dynamical variables of the laser [15]. However, quantum noise [3,25] that is naturally present in all lasers has not been considered so far. In this paper we show that quantum noise in spite of its weakness is sufficient to drive modal fluctuations comparable to those observed in experiments. No additional excitation is then required for the numerical simulation of laser dynamics.

The number of frequencies in the spectrum of modal fluctuations, i.e., the number of relaxation modes, can be as large as the number of oscillating light modes [26]. Modal fluctuations at the highest frequency are correlated. They represent the well-known relaxation oscillations of the total laser output. Modal fluctuations at lower frequencies are anticorrelated and they may completely cancel in the total output. For a large number of oscillating modes low-frequency relaxation oscillations are expected to disappear from the laser

dynamics [26]. However, so far all experiments have been performed with short-cavity lasers and with homogeneously broadened gain media. The number of oscillating longitudinal modes in these lasers is relatively small ($\mathcal{N} < 10$) and allows easier modeling and numerical simulations of laser dynamics. The opposite case of a large number of longitudinal lasing modes ($\mathcal{N} \gg 1$) is also important. Such lasers are applied, e.g., for sensitive intracavity absorption measurements [1] and for noise suppression by intracavity second-harmonic generation [27]. There are some specific features in these multimode lasers that lead to significant simplifications and make it possible to derive an analytical solution of the corresponding laser equations [28,29].

In this paper we investigate a multimode laser ($\mathcal{N} > 10$) with a chip of Nd^{3+}-doped glass used as the active medium instead of a crystal. The large contribution of inhomogeneous spectral broadening of the gain allows us to excite laser oscillation in more than 100 longitudinal modes even if the cavity is only a few millimeters long. Instead of spectral narrowing observed with homogeneously broadened lasers [1], the emission spectrum of these lasers broadens with the time after the pump power is switched on [30].

Resonance peaks in the fluctuation spectra of the individual modes and of the total output as well as correlations of various laser modal fluctuations are investigated and compared to the results for lasers with only a few modes. Observed fluctuations of emission in the laser modes in the cw regime are well reproduced by numerical simulations, including quantum noise.

This paper is organized in the following way. Section II outlines the experimental setup and the results of the measurements. A theoretical model based on rate equations supplemented by Langevin forces is introduced in Sec. III. The results of numerical simulations are given in Sec. IV. Analytical estimations of the frequencies of antiphase oscillations in the output of individual modes of multimode lasers is presented in Sec. V. The principal results are summarized in Sec. VI.

II. EXPERIMENT

A. Experimental setup

The experimental setup is shown in Fig. 1. The multimode laser is made out of a 4-mm-thick disk of Schott LG680 silicate-based laser glass, doped with 3% (by weight) of Nd. The Nd:glass is mounted in a thermoelectrically cooled copper housing. The lifetime of the upper laser level is $\tau_u = 0.29$ ms. Both sides of the disk are coated with dielectric mirrors M1 ($R = 10\%$ at 810 nm and $R \cong 100\%$ at 1060 nm) and M2 ($R = 99\%$ at 1060 nm). The optical length of the cavity is 6 mm. The Nd:glass laser is optically pumped through the mirror M1 by the output of a cw Ti:sapphire laser (Spectra Physics, Model 3900S) at 810 nm focused into the disk with lens L1 ($f = 40$ mm). The threshold pump power of the disk laser is 140 mW. The pump power is monitored by a Si photodiode PD1. The Ti:sapphire laser is optically pumped at 532 nm by MilleniaV-laser (Spectra Physics). An acousto-optical deflector (AOD1) is used for step modulation of the pump power between 100% and 25%
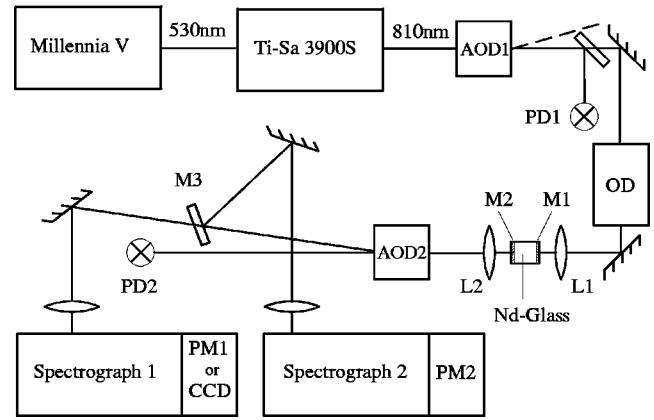

FIG. 1. Experimental setup.

of the initial level. An optical isolator is used to attenuate by 30 dB the light reflected from various optical components back into the Ti:sapphire laser.

The output light of the Nd:glass laser is collimated by lens L2 ($f = 60$ mm) and divided into two beams by AOD2. The direct beam is used for measuring the total power of the laser by a Si photodiode PD2. The deflected beam is split again into two beams by a 50% beam-splitter M3 for spectrally resolved correlated two-channel recording. These two beams are spectrally analyzed with two grating spectrographs whose intervals of spectral resolution are 5 GHz (Spectrograph 1) and 1 GHz (Spectrograph 2). This spectral resolution is sufficient to resolve the individual longitudinal laser modes, which are separated in our experiment by 10 GHz. Equipped with photomultipliers PM1 and PM2, the spectrographs are used as monochromators for simultaneous recording of the emission in two different laser modes with 1-MHz time resolution. Alternatively spectrograph 1 was equipped with a 17.28-mm-long charge-coupled device (CCD) (1728 channels, Thomson CSF TH 7803) for recording the entire emission spectrum of the laser. The time resolution of such spectral recording is set by AOD2. The recorded signals are stored in a two-channel digital oscilloscope with 10-bit dynamical and 10-MHz time resolution (Krenz TRB4000).

B. Spectral dynamics

Emission spectra of the Nd:glass laser recorded by the CCD array at different times t after the onset of laser oscillations are shown in Fig. 2. The pump rate normalized to the laser threshold in these records is $\eta = P/P_{th} = 1.64$. The emission spectra consist of many peaks corresponding to individual longitudinal laser modes, which are well resolved in the records. Initially, the emission dynamics is determined by inhomogeneous spectral broadening of the gain caused by nonequivalent locations of the active Nd ions in the glass matrix [29–31]. The laser starts oscillating in the modes with the highest net gain, depleting their inversion. Due to the inhomogeneity, the inversion of the spectrally neighboring modes is not depleted and their gain continues to grow until their lasing thresholds are reached, and these modes begin oscillating. At 35 to 60 μs after the onset of laser oscillations, two neighboring mode groups, spectrally separated
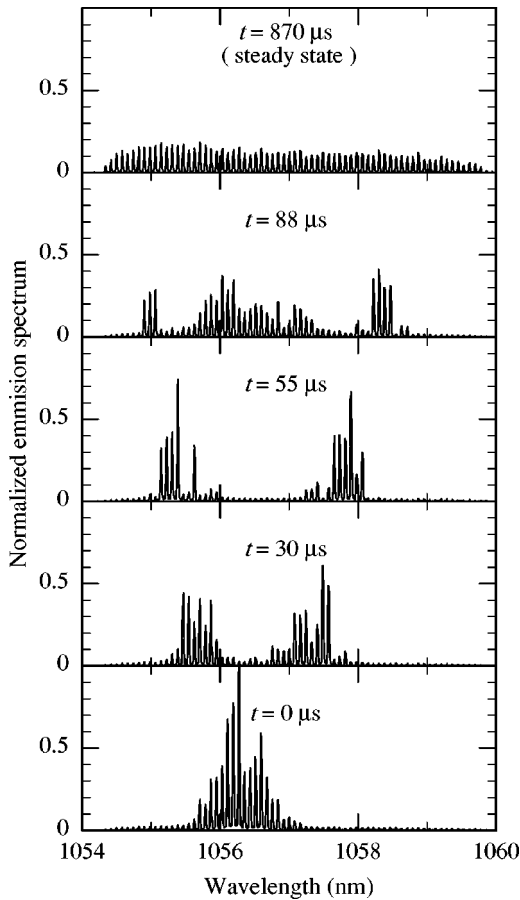
FIG. 2. Emission spectra of a Nd:glass laser recorded at five different times t after the onset of laser oscillations normalized to the maximum peak at $t=0$. The sequence of spectra represents damped waves in the spectral dynamics.

FIG. 3. Emission spectra of a cw Nd:glass laser recorded at four different pump rates η. Each emission spectrum is normalized to its maximum value. $\mathcal{N}$ is the number of oscillating laser modes.

C. Relaxation oscillations

In cw operation the total laser power and the power in individual laser modes show characteristic fluctuations around their mean values as it is demonstrated in Fig. 4 for $\eta=1.19$. The emission in an individual laser mode (bottom) has been selected by the spectrograph and recorded simulta-

from the initially oscillating central modes approximately by one homogeneous linewidth, $\Delta \nu_{hom} \cong 30$ cm^{-1} [31], dominate the emission spectrum of the laser. At 93 μs, the emission of these neighboring groups of modes has almost vanished, whereas the central modes and more distant modes appear in the laser spectrum. The alternation of the emission of neighboring mode groups gives rise to transient spectral waves in the laser emission propagating from the center to the edges of the spectrum. In cw operation these waves are damped, and the spectral width of the emission spectrum is determined by the spectral width of the laser gain, and by the pump rate. With increasing pump rate the gain in the central modes becomes saturated, whereas the gain in the distant groups of laser modes keeps growing until their thresholds are reached. As a result the number of oscillating modes $\mathcal{N}$ increases with the pump rate, which is demonstrated in Fig. 3. This is in contrast to what is observed in a laser with homogeneously broadened gain that is not affected by the increasing pump rate and leaves the emission spectrum narrow. Therefore, a glass laser is a suitable medium for studying the dynamics of lasers with a large number of oscillating modes.
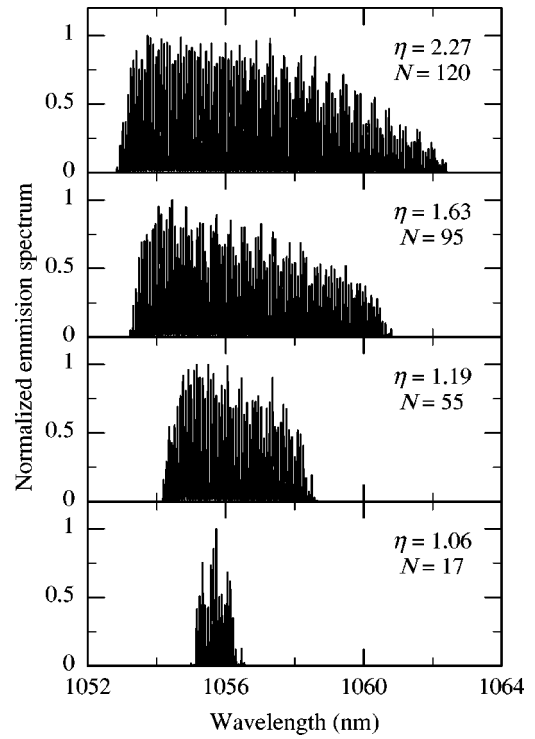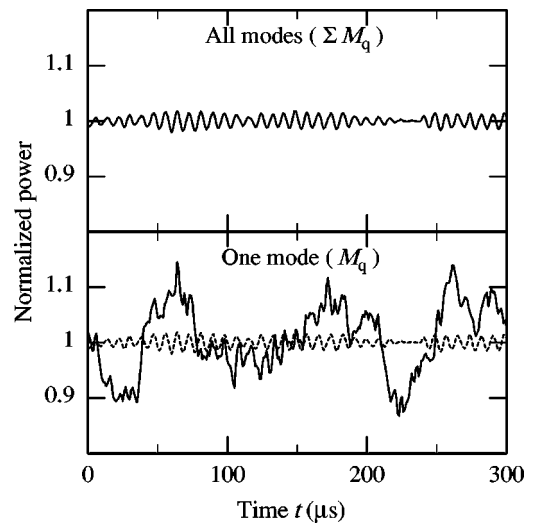

FIG. 4. Amplitude fluctuations of the total laser power (top) and of the power in one individual mode (bottom), recorded simultaneously at $\eta=1.19$. Emission power is normalized to the corresponding mean value. Total power is additionally shown in the bottom diagram by the dashed line.
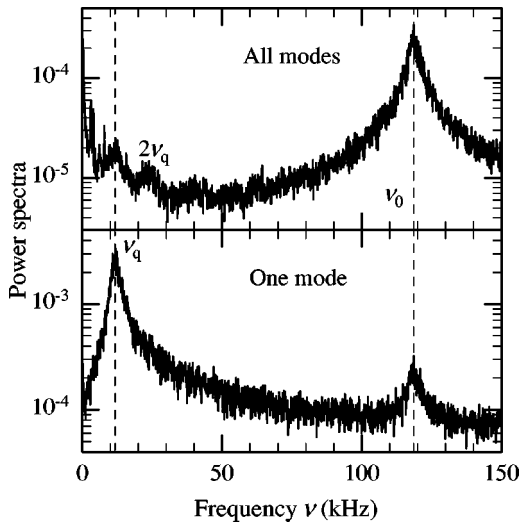
FIG. 5. Low-frequency power spectra of the total (top) and of the modal (bottom) power calculated from experimental records of laser emission at $\eta = 1.19$ and normalized to the zeroth Fourier component. Frequency positions of in-phase (ν_0) and antiphase (ν_q) relaxation oscillations are shown by dashed lines.

neously with the total power (top) by a two-channel digital oscilloscope. In the fluctuations of the individual laser mode (bottom), one recognizes two types of oscillations: (i) in-phase oscillations of all modes with a characteristic time scale of ≈ 10 μs and an amplitude of up to 3%, and (ii) antiphase oscillations with a characteristic time scale of ≈ 100 μs and an amplitude of up to 15%. The total laser power does not show slow oscillations of the second type, confirming the perfect cancellation of these oscillations in different laser modes. In contrast, the fast oscillations of the total laser power (first type), show the same amplitude as oscillations in individual modes, proving their in-phase nature.

Figure 5 shows the power spectra of the observed fluctuations of the total output (top) and of the output in one of the central laser modes at $\eta = 1.19$. They are Fourier transformations of long (≈ 64 ms) experimental records and are normalized to their component at zero frequency. Therefore, all power spectra show fluctuation amplitudes relative to the corresponding mean power and are compatible. In previous experiments with a small number of oscillating modes [15–17] power spectra of the modal intensities revealed many low-frequency peaks. The number of these peaks was observed to be as large as the number of modes $\mathcal{N}$ oscillating in the laser. In the present experiment spectra of the modal powers show only two peaks, one at the frequency ν_0 of in-phase oscillations and another one, 10 times stronger, at the frequency ν_q of antiphase oscillations, which depends upon the modal power. Fluctuations of the total laser power (Fig. 5, top) are much weaker than fluctuations of the modal power (Fig. 5, bottom) since the dominant fluctuations are antiphase oscillations that cancel in the total output. The power spectrum of the total output reveals just weak residual oscillations at ν_q with less than 1% of the amplitude of antiphase modal oscillations.
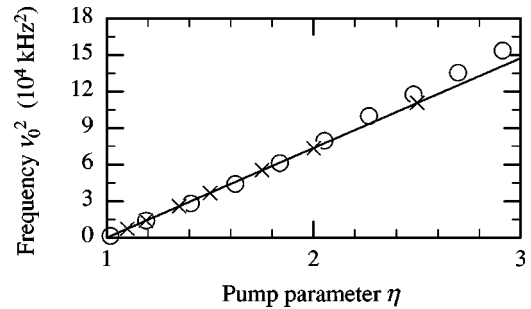

FIG. 6. Square of the frequency of in-phase relaxation oscillations ν_0^2 vs pump rate η measured in the experiment (circles) and found from computer simulations (crosses). The line is a linear fit over the first six experimental points.

In the total output also oscillations at $2\nu_q$ show up. These second-harmonics oscillations are very weak and are not clearly visible in the modal power because of the strong and broad peak at the fundamental frequency, ν_q. However, in the total output the second-harmonics oscillations are not compensated and appear almost as strong as oscillations at ν_q.

The strongest fluctuations of the total laser power take place at the frequency of the in-phase oscillations ν_0. The relative amplitudes of these oscillations in the total and modal laser power are about the same (2×10^{-3}). Narrow peaks below 5 kHz and background noise in Fig 5 are caused by fluctuations in the pump power.

Figure 6 shows positions of the frequencies ν_0 of in-phase relaxation oscillations measured at different pump rates. At a moderate pump rate, the emission spectrum of the Nd:glass laser is relatively narrow and the dependence $\nu_0(\eta)$ corresponds to the case of a laser with homogeneously broadened gain [32],

$$2\pi\nu_0 = \sqrt{\gamma A(\eta - 1)}, \qquad (2.1)$$

where γ is the cavity-loss rate and A is the decay rate of the upper laser level. The frequencies of these relaxation oscillations at high pump rates are slightly larger than expected from Eq. (2.1). This deviation is caused by increasing the cavity loss from the thermal distortion of the glass at high pump power, and by the increasing contribution of inhomogeneous line broadening. The linear fit of the experimental data to Eq. (2.1) in Fig. 6 uses the first six data points only. From this fit, and with the known value of the lifetime of the upper laser level, $\tau_u = 290$ ms ($A = 3.45 \times 10^3$ s^{-1}), we estimate the actual cavity-loss rate to be $\gamma = 8.45 \times 10^8$ s^{-1}, which corresponds to 3.3% loss per cavity round trip.

In contrast to the in-phase oscillations at ν_0, antiphase oscillations of the modal power at ν_q depend only on the mean modal power, but not on the total power of the laser. Figure 7 shows positions of ν_q measured at different pump rates in one of the central modes. The mean modal power does not increase linearly with the pump rate, since the number of oscillating modes also depends upon the pumping. Therefore, Fig. 7 shows the dependence of ν_q upon modal power, but not on the pump rate, as in Fig. 6. The accuracy of measurements of the absolute modal power in the experi-
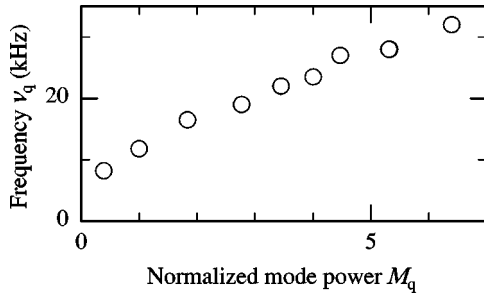
FIG. 7. Frequency of antiphase relaxation oscillations ν_q measured in one of the central modes vs modal power M_q, normalized to the second data point.

ment was lower than that of the relative modal power. For this reason relative values of the modal power are used in Fig. 7; they are normalized to the value of the modal power at the second data point.

D. Polarization dynamics

Since the facets of the Nd-doped glass are coated directly with mirrors, there is no selection of polarization, and the laser generally emits elliptically polarized light. Spatial inhomogeneity of the gain in the azimuthal direction gives rise to antiphase oscillations of polarization modes [20]. This phenomena is also present in our experiment. Figure 8 shows the emission in two orthogonal polarizations, measured with a polarizer in front of the photodiode PD2 in Fig. 1. As in Fig. 4 notice fast in-phase oscillations at ν_0, and slow antiphase oscillations at frequency ν_{pol}. Figure 9 shows power spectra of the total output at each polarization. The records of the emission at the two polarizations in Fig. 8 are not synchronized, therefore the antiphase character of slow oscillations does not show up in the diagrams. However, when the polarizer is removed a slow frequency component at ν_{pol} vanishes almost completely, as can be seen from a comparison of Figs. 5 and 9. The absolute amplitude of the observed polarization

FIG. 9. Power spectra of the laser power emitted in two polarizations, calculated similarly to Fig. 5.

oscillations is the same for both polarizations. However, the relative amplitude differs since the mean power in the two polarizations is different.

E. Mode correlations

Antiphase modal dynamics is characterized by the compensation of the oscillations in one individual mode by the rest of modes, so that these oscillations disappear in the total laser output. In order to find out how this compensation is distributed in the spectrum, the outputs of two particular laser modes have been recorded simultaneously using both spectrographs shown in Fig. 1. As an example, Fig. 10 shows the laser power emitted in two neighboring modes. In order to see the strength of correlation between different pairs of modes we have calculated their correlation functions according to
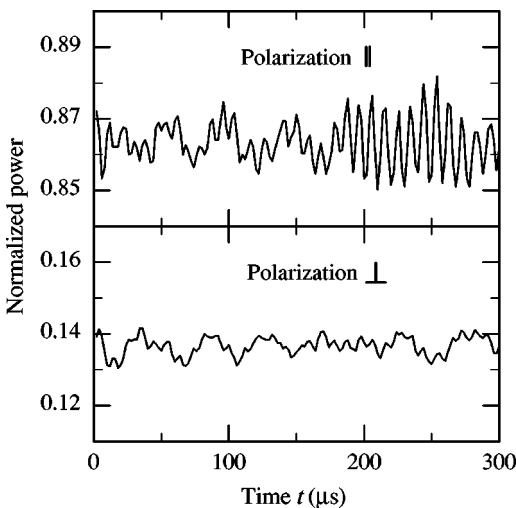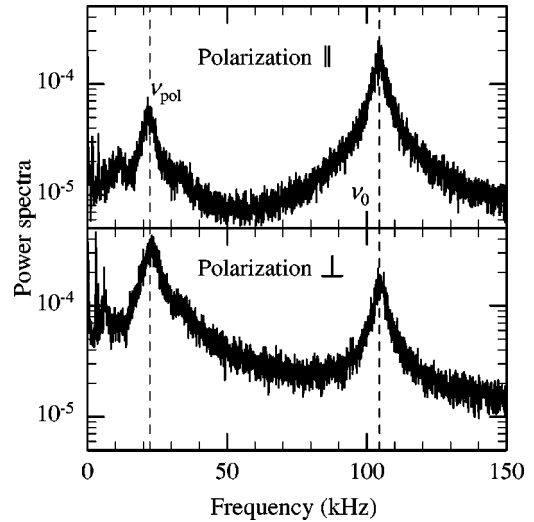

FIG. 8. Laser intensity measured in two orthogonal polarizations. The power in each polarization is normalized to the mean total power and not synchronized.
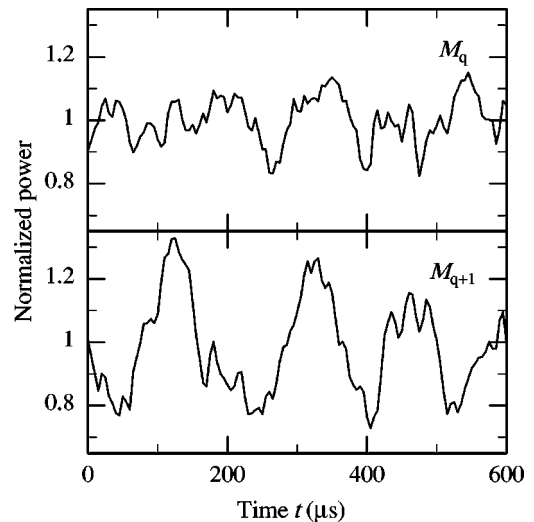

FIG. 10. Simultaneously recorded power of two neighboring laser modes, M_q and M_{q+1}. Each record is normalized to its mean power.
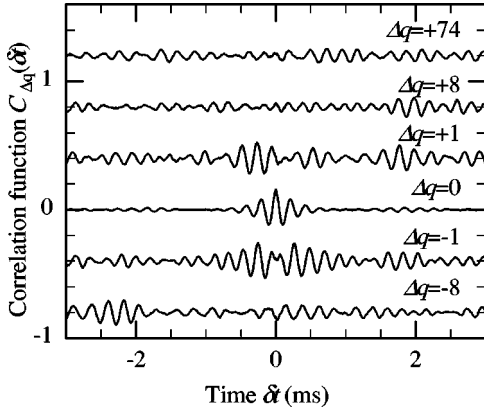
FIG. 11. Correlation function $C_{\Delta q}(\delta t)$ of the central mode recorded in the experiment with other modes separated by Δq mode spacings. Positive values of Δq indicate an increase of the optical frequency of the laser mode. The autocorrelation function ($\Delta q = 0$) is scaled down by a factor of 4; correlation functions at $\Delta q \neq 0$ are shifted successively along the y axis.

$$C_{\Delta q}(\delta t) = \frac{\langle (M_q - \langle M_q \rangle)(M_{q+\Delta q}(t+\delta t) - \langle M_{q+\Delta q} \rangle) \rangle}{\langle M_q - \langle M_q \rangle \rangle \langle M_{q+\Delta q} - \langle M_{q+\Delta q} \rangle \rangle}.$$
(2.2)

Figure 11 shows the calculated from the experimental data correlation function of one of the central laser modes with other modes separated by Δq mode spacings in both directions in the spectrum. These data show that the correlation between laser modes decreases as their spectral separation increases. Strong correlation exists only in the group of neighboring modes of about the same amplitude. That means that low-frequency oscillations at frequencies ν_q in individual modes are compensated via antiphase oscillations only in the neighboring modes. As a result, the low-frequency spectrum of modal intensity shows only one or maybe just a small number of overlapped relaxation oscillation frequencies corresponding to antiphase oscillations in the neighboring modes. Oscillations at other frequencies, corresponding to distant modes of different amplitudes, are very weak and they do not appear in the spectrum (see Fig. 5).

III. THEORETICAL MODEL

A. Rate equations

In order to explain the experimental observations, and especially the cw emission dynamics, we shall use rate equations for a multimode laser including spatial inhomogeneity [18], inhomogeneous pumping along the cavity [19], and Langevin forces modeling quantum noise [25],

$$\frac{d}{dt}M_q(t) = B_q(M_q+1)\int_0^L dz\,[\psi_q(z)N(z)] - \gamma M_q + F_q,$$
(3.1)

$$\frac{\partial}{\partial t}N(z,t) = P(z) - AN(z) - \sum_q B_q M_q \psi_q(z)N(z) + F_N(z).$$
(3.2)

Here M_q is the photon number in the axial laser mode q with distribution $\psi_q(z)$ along the optical axis of the cavity ($z=0$ is the position on the optical axis at mirror M1), B_q is the gain rate per one inverted ion and one photon in mode q, γ is the cavity-loss rate assumed to be equal for all modes, L is the resonator length, $N(z)$ and $P(z)$ are the inversion and pump rate densities per cavity length, respectively, and A is the decay rate of the upper laser level. F_q and $F_N(z)$ are Langevin forces describing the quantum noise of the photon number in the cavity and inversion, respectively. Their definition is given in Sec III C. The variables M_q, $N(z)$, F_q, and $F_N(z)$ are always functions of time, which is not always explicitly written.

In a cavity of the Fabry-Perot type the axial power distribution ψ_q of the modal power is

$$\psi_q(z) = 1 - \cos(k_q z) \quad \text{with} \quad k_q = \frac{2\pi q}{L}.$$
(3.3)

Rate equations (3.1) and (3.2) can be simplified by Fourier expanding the spatial dependence in terms of modal functions. Fourier components of the laser inversion, pump power, and Langevin forces are calculated according to

$$N(z,t) = N_0 + 2\sum_{i=1/2,1,\ldots}^{\infty} N_i \cos(k_i z),$$
(3.4)

$$N_i(t) = \frac{1}{L}\int_0^L dz\, N(z,t)\cos(k_i z),$$
(3.5)

$$P(z,t) = P_0 + 2\sum_{i=1/2,1,\ldots}^{\infty} P_i \cos(k_i z),$$
(3.6)

$$P_i(t) = \frac{1}{L}\int_0^L dz\, P(z,t)\cos(k_i z),$$
(3.7)

$$F_N(z,t) = F_{N_0} + 2\sum_{i=1/2,1,\ldots}^{\infty} F_{N_i}\cos(k_i z),$$
(3.8)

$$F_{N_i}(t) = \frac{1}{L}\int_0^L dz\, F_N(z,t)\cos(k_i z).$$
(3.9)

Here N_0, P_0, and F_{N_0} are mean values of the laser inversion, pump power, and Langevin forces in the cavity, respectively. With the power distribution (3.3) and the Fourier expansions (3.4)–(3.9), the rate equations (3.1) and (3.2) become

$$\frac{d}{dt}M_q(t) = B_q(M_q+1)L(N_0-N_q) - \gamma M_q + F_q,$$
(3.10)

$$\frac{d}{dt}N_i(t) = P_i - N_i\left(A + \sum_q B_q M_q\right)$$

$$+ \sum_q \frac{B_q M_q}{2}(N_{q+i} + N_{|q-i|}) + F_{N_i}.$$
(3.11)

In these equations the index q is the number of standing half-waves of mode q in the cavity, $q = 2L/\lambda_q$. It takes $\mathcal{N}$ different values corresponding to all lasing modes. Index i, in addition to all values of q, includes the zero Fourier components $i = 0$ describing corresponding mean quantities. Indices i with half-integer values in Eqs. (3.4)–(3.9) disappear after integrating over the cavity length. Equation (3.10) shows that the modal power is affected only by the corresponding inversion component N_q. However, each inversion component is affected by other laser modes and inversion components as well. Mixed terms $\Sigma_q (B_q M_q/2)(N_{q+i} + N_{|q-i|})$ in Eq. (3.11) consist of high, N_{q+i}, and low, $N_{|q-i|}$, spatial frequencies. In the following numerical calculations we use equations including just the strongest components of the inversion, N_q, and, if necessary, the high and the low Fourier components of the inversion. The latter one is important in the case of inhomogeneous distribution of the pump power along the cavity, e.g., when the gain medium fills only a part of the cavity, or if the absorption length of the pump is shorter than the cavity [19]. In this case, the Fourier components of pumping are in resonance with low-frequency components of the inversion.

B. Normalized variables

The stationary inversion $N_{0,th}$ at laser threshold, when stimulated emission compensates the loss only in the mode q_0 with the highest gain B_{q_0}, is calculated from Eq. (3.10) with spontaneous emission neglected as

$$N_{0,th} = \frac{\gamma}{B_{q_0}L}. \tag{3.12}$$

The pump rate $P_{0,th}$ required to reach the laser threshold in the mode q_0 is calculated with Eqs. (3.11) and (3.12) as

$$P_{0,th} = \frac{A\gamma}{B_{q_0}L}. \tag{3.13}$$

In order to generalize the results for various types of lasers we introduce normalized variables

$$\eta_i = P_i/P_{0,th}, \tag{3.14}$$

$$n_i = N_i/N_{0,th}, \tag{3.15}$$

$$b_q = B_q/B_{q_0}, \tag{3.16}$$

$$m_q = M_q B_{q_0}/A, \tag{3.17}$$

$$\tau = At, \tag{3.18}$$

$$G = \gamma/A. \tag{3.19}$$

Including these variables in Eqs. (3.10) and (3.11) we obtain the normalized rate equations

$$\frac{d}{d\tau}m_q(\tau) = G\left[b_q\left(m_q + \frac{B_{q_0}}{A}\right)(n_0 - n_q) - m_q\right] + F_q\frac{B_{q_0}}{A^2}, \tag{3.20}$$

$$\frac{d}{d\tau}n_i(\tau) = \eta_i - n_i\left(1 + \sum_q b_q m_q\right) + \sum_q \frac{b_q m_q}{2}(n_{q+i} + n_{|q-i|})$$

$$+ \frac{F_{N_i}}{N_{0,th}A}. \tag{3.21}$$

C. Langevin forces

Generally, rate equations describe the averaged dynamics of lasers. For instance, the loss rate in the cavity mode q is represented by the mean value γM_q. However, in a particular laser this rate fluctuates. The same is true for the stimulated emission, for pumping, and for the decay of the inversion. The reason for these fluctuations is quantum noise appearing from the quantization of light-atom interaction. Quantum noise can be satisfactorily modeled in the rate equations by introducing stochastic Langevin forces [3,25]. The amplitudes of the Langevin forces are normalized as

$$\langle F_q(t)\rangle = 0, \tag{3.22}$$

$$\langle F_N(z,t)\rangle = 0, \tag{3.23}$$

$$\langle F_q(t)F_q(t')\rangle = \left[B_q(M_q+1)\int_0^L dz\,\psi_q(z)N(z) + \gamma M_q\right]$$

$$\times \delta(t-t'), \tag{3.24}$$

$$\langle F_N(z,t)F_N(z',t')\rangle = \left[P(z) + AN(z)\right.$$

$$\left. + \sum_q B_q M_q \psi_q(z)N(z)\right]\delta(t-t')$$

$$\times \delta(z-z'). \tag{3.25}$$

With these forces all of the above rates become Poisson distributed around their mean values. For simplicity we did not take into account possible correlations between different parts of the Langevin forces, e.g., correlation of the fluctuations of laser inversion and photon numbers in laser modes due to stimulated emission.

The Fourier components of the Langevin force for the laser inversion, required for Eq. (3.21), are calculated by using Eq. (3.25),

$$\langle F_{N_i}(t)F_{N_j}(t')\rangle = \frac{4}{L^2}\int_0^L dz\int_0^L dz'[\cos(k_i z)\cos(k_j z')$$

$$\times \langle F_N(z,t)F_N(z',t')\rangle] \tag{3.26}$$

$$= \frac{1}{L} \delta(t-t') \Bigg\{ P_{i+j} + P_{|i-j|} + A(N_{i+j} + N_{|i-j|})$$

$$+ \sum_q B_q M_q \Bigg[N_{i+j} + N_{|i-j|} + \frac{1}{2}(N_{i+j+q} + N_{|i-j+q|}$$

$$+ N_{|i+j-q|} + N_{|i-j-q|}) \Bigg] \Bigg\}. \tag{3.27}$$

The zeroth Fourier components of the distribution of pumping and inversion along the cavity are much larger than all other components if the pumping distribution is reasonably smooth. In the following all nonzero components in Eq. (3.27) will be neglected. Taking into account that the mixed terms $\langle F_{N_i}(t) F_{N_j}(t') \rangle$ have zero Fourier components only if $i=j$, Eq. (3.27) simplifies into

$$\langle F_{N_i}(t) F_{N_j}(t') \rangle \approx \frac{\delta_{i,j}}{L} \delta(t-t') \Bigg(P_0 + A N_0 + \sum_q B_q M_q N_0 \Bigg). \tag{3.28}$$

With Eqs. (3.24) and (3.28) the rate equations (3.20) and (3.21) for the normalized variables can be written as

$$\frac{d}{d\tau} m_q(\tau) = G \Bigg[b_q \Bigg(m_q + \frac{B_{q_0}}{A} \Bigg)(n_0 - n_q) - m_q \Bigg]$$

$$+ \sqrt{ \frac{B_{q_0} G}{A} \Bigg[b_q \Bigg(m_q + \frac{B_{q_0}}{A} \Bigg)(n_0 - n_q) + m_q \Bigg] } \, \xi_q(\tau), \tag{3.29}$$

$$\frac{d}{d\tau} n_i(\tau) = \eta_i - n_i \Bigg(1 + \sum_q b_q m_q \Bigg) + \sum_q \frac{b_q m_q}{2} (n_{q+i} + n_{|q-i|})$$

$$+ \sqrt{ \frac{1+\delta_{0,i}}{N_{0,s} L} \Bigg[\eta_0 + n_0 + \sum_q b_q m_q (n_0 + n_q) \Bigg] } \, \xi_{N_i}(\tau), \tag{3.30}$$

where $\xi_i(\tau)$ is a stochastic variable with $\langle \xi_i(\tau) \rangle = 0$ and $\langle \xi_i(\tau) \xi_j(\tau') \rangle = \delta_{i,j} \delta(\tau - \tau')$.

IV. NUMERICAL SIMULATION

The laser dynamics has been simulated by calculating Eqs. (3.29) and (3.30) with laser parameters A, L, G, B_{q_0}, b_q, and η_i taken from the experiment. The decay rate of the population on the upper laser level, $A = 3.45 \times 10^3$ s^{-1}, is taken from the data sheet on silicate glass LG680 supplied by Schott. The optical length of the cavity is set to the experimental value of $L = 6$ mm. The cavity loss rate γ and the parameter G [Eq. (3.19)] are found from the experiment using Eq. (2.1). With the data in Fig. 6 we obtain $G = 2.45 \times 10^5$. The gain rate is calculated from the output power of the laser I measured at a particular pump rate η according to

$$B_{q_0} = \frac{A(\eta-1)Tc^2 h}{2L\lambda I}, \tag{4.1}$$

where T is the transmission of the output mirror (1%), c is the velocity of light, h is Planck's constant, and λ is the wavelength of laser emission. The expression (4.1) is derived from the stationary solution of the simplified rate equation (3.11) for the mean value of the inversion N_0 ($i=0$) and without the Langevin force. With 20.5-mW output at $\eta = 1.6$ we get $B_{q_0} = 4.7 \times 10^{-6}$ s^{-1}.

The spectral dependence of the gain is approximated by a Lorentzian profile

$$B_q = B_{q_0} \frac{1}{1 + \left[\dfrac{\delta B}{B_{q_0}} (q-q_0) \right]^2}, \tag{4.2}$$

where q is the mode number, and q_0 the central mode. The reduction of gain, δB, outside the center of the emission spectrum is adjusted individually for each pumping level to have the same number of oscillating modes in the simulations as in the experiment. This corresponds to adjusting the width of the homogeneous gain profile in order to simulate a broad emission spectrum (see Fig. 3).

In the experiment, the active medium fills the entire resonator. Thus, the pump power distribution decays exponentially along the laser axis resulting from the 90% pump absorption in the glass. A Fourier transform of this distribution provides a rapidly declining series of values $\eta_1 > \eta_2 > \cdots > \eta_i$ so that only the lowest-order ones need to be taken into account.

The largest number of modes assumed oscillating in our simulations was $\mathcal{N} = 55$ and the time increment 10^{-9} s. Two types of simulations were made: The first type took into account only the Fourier components N_q of the inversion directly corresponding to the laser modes q and assuming a homogeneous pump distribution (only one component of pump, η_0, is present). The second type includes, in addition, Fourier components of the inversion $N_1, \ldots, N_{\mathcal{N}-1}$ at difference frequencies and $N_{2q_0-(\mathcal{N}-1)}, \ldots, N_{2q_0+(\mathcal{N}-1)}$ at sum frequencies, and the first Fourier components $\eta_1, \ldots, \eta_{\mathcal{N}-1}$ of pump power distribution.

Figure 12 shows total (top) and modal (bottom) laser powers obtained in the simulations of the first type, with the same values of the laser parameters as present in the experiment of Fig. 4 (cw regime at $\eta = 1.19$ and $\mathcal{N} = 55$). All characteristic properties of the experimental results are well reproduced in the simulation. Quantum fluctuations turn out to be strong enough to excite large scale antiphase oscillations in individual laser modes. In both simulation and experiment, these fluctuations cancel in the total output such that only residual, in-phase oscillations of smaller amplitude and at the highest frequency survive.

Figure 13 shows Fourier spectra obtained from the simulations shown in Fig. 12 for the total (top) and modal (bottom) laser output. As in the experiment, the low-frequency spectrum of the modal power shows two peaks: one at the frequency ν_0 of in-phase oscillations and another, ten-times stronger, at the frequency ν_q of antiphase oscillations. Notice, in addition, two small peaks at the second harmonic $2\nu_q$ and at the difference frequency $\nu_0 \pm \nu_q$. The observed spec-
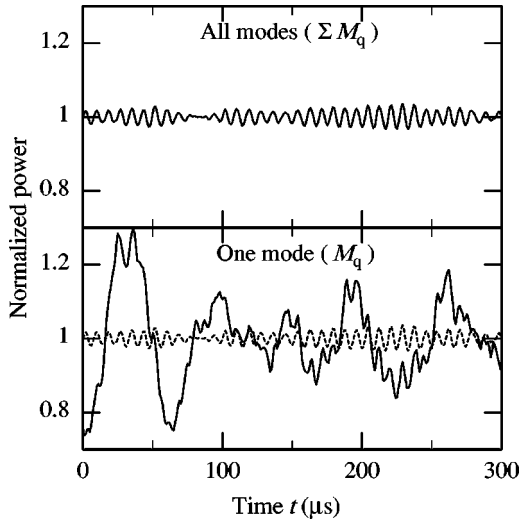
FIG. 12. Amplitude fluctuations of the total (top) and modal laser power (bottom) obtained from simulations. The emission power is normalized to the corresponding mean value. The total power is presented for comparison in the bottom diagram by the dashed line.

tral peaks in the simulation are higher and narrower than in the experiment. The amplitude of the fluctuations in the simulations is also somewhat larger than in the experiment. This reason for that might be insufficient spectral resolution of the experiment.

In previous experiments with a small number of oscillating modes ($\mathcal{N}<10$) [15–17] power spectra of modal intensities have revealed as many low-frequency peaks as the number of oscillating modes $\mathcal{N}$. In order to reproduce these results and to study the transition between the regime with single and several distinguishable frequencies of antiphase oscillation we have simulated the laser dynamics with a dif-
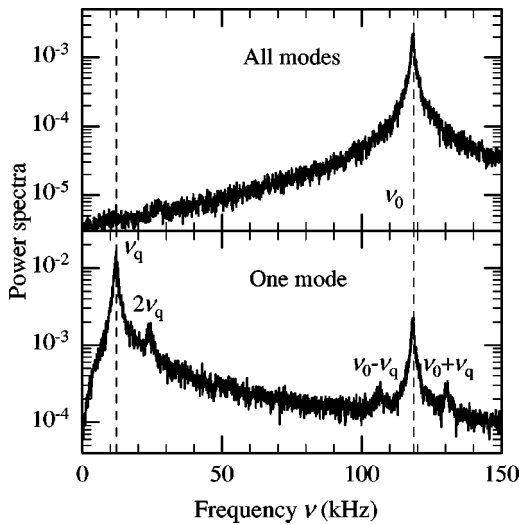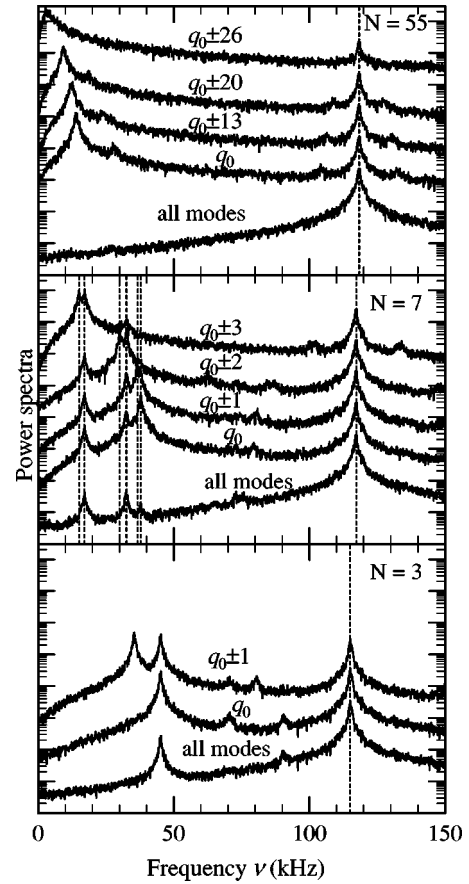

FIG. 14. Low-frequency spectra of the total power and of the power in different individual modes obtained in simulations ($\eta = 1.19$) with different numbers of oscillating modes $\mathcal{N}$. Neighboring curves are separated by one order of magnitude offset. Frequency positions of in-phase (ν_0) and antiphase (ν_q) relaxation oscillations are shown by dashed lines for $\mathcal{N}=55$.

ferent number of modes. Figure 14 shows power spectra of simulated laser dynamics with $\mathcal{N}=3,7$, and 55. In these simulations the pump rate was kept constant, but the gain width was varied. The power spectra of simulations with the total mode number $\mathcal{N}=3$ shows three well-resolved peaks corresponding to compensated and uncompensated oscillations, as expected. With $\mathcal{N}=7$ seven different oscillation frequencies appear in the modal power. They are not all well resolved, but are marked in Fig. 14 by vertical dashed lines. The frequencies are divided in groups of two, with one frequency of compensated oscillations that are present only in two modes symmetric to the center and another frequency of in-phase oscillations shared by all modes and by the total output. Each mode has its preferred oscillation frequency with the highest peak. With $\mathcal{N}=55$ these individual peaks become dominant, whereas oscillations at other frequencies disappear. Only one in-phase oscillation remains in the spectrum of the total power. Its frequency ν_0 increases slightly with the number of oscillating modes growing. This tendency indicates better depletion of the inversion and higher efficiency when more modes are oscillating.

The frequency of the in-phase oscillations obtained from simulations is shown as a function of the pump rate together

FIG. 13. Low-frequency power spectra of the total (top) and of the modal (bottom) power obtained in simulations ($\eta=1.19$, $\mathcal{N} = 55$), and normalized to the zeroth Fourier component. Frequency positions of in-phase (ν_0) and antiphase (ν_q) relaxation oscillations are shown by dashed lines.
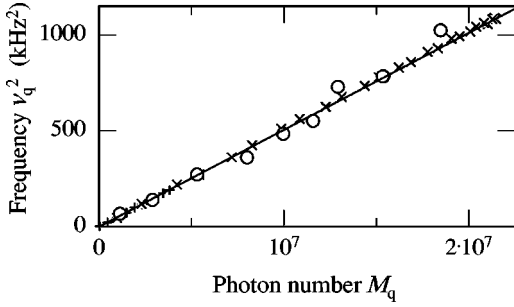
FIG. 15. Square of the frequency of antiphase relaxation oscillations ν_q measured in the modal power of the laser (circles) and obtained from numerical simulations (crosses) vs photon numbers in laser modes. The straight line shows the dependence given by Eq. (5.13).

FIG. 16. Correlation function of one simulated laser mode with other modes separated by Δq mode spacings. Positive values of Δq indicate an increase of the optical frequency of the laser mode. The autocorrelation function ($\Delta q = 0$) is scaled down by a factor of 4; other correlation functions ($\Delta q \neq 0$) are shifted successively along the y axis.

with the experimental results in Fig. 6. As expected, the simulated results overlap perfectly with the fit line used to calculate the cavity loss γ and the parameter G. The mode number in these simulations was varied from 7 to 55.

In contrast, the frequency of the antiphase relaxation oscillation ν_q is different for each mode and depends upon the power in this mode only, but not upon the total power. Figure 15 shows the dependence of the square of this frequency upon the modal power obtained from numerical simulations (crosses) in comparison to the experimental data from Fig. 7 (circles). Laser dynamics was simulated at $\eta = 1.23$ with $\mathcal{N} = 55$ modes, and at $\eta = 1.5$ with $\mathcal{N} = 25$ modes. The Lorentzian gain profiles were adjusted such that the modes far from the center were very weak and the number of photons in all the modes is spread over a large range sufficient to present the dependence $\nu_q^2(M_q)$ in Fig. 15. The photon numbers of laser modes in the experiment of Fig. 7 are measured with high relative, but low absolute, accuracy. Therefore, the power at one experimental point (third point with $\nu_q = 19$ kHz) is normalized to the photon number in the laser mode showing the same oscillation frequency in numerical simulations. Taking into account that the total laser output in that measurement was 19 mW ($\eta = 1.6$) and the total number of oscillating modes $\mathcal{N} \cong 95$, the estimated photon number in the experiment was $(4.3 \pm 50\%) \times 10^6$. This value compares rather well with the value $M_q = 7.17 \times 10^6$ taken as a reference in the simulations. The main phenomenon demonstrated in Fig. 15 is that the values ν_q^2 plotted vs the mode power in the simulation as well as in the experiment perfectly fit to a straight line.

In the results presented above no essential difference was found when using the two different types of simulations. However, some other features, e.g., the stationary emission spectrum of the laser [33] or the mode correlation functions, are modified when using nonuniform pumping and include difference and sum Fourier frequencies of inversion in the simulations. Figure 16 shows the correlation function $C_{\Delta q}(\delta t)$ of one of the laser modes from a type-2 simulation with other modes separated by a varying number of mode spacings, Δq. As in the experiment (see Fig. 11), the correlation function decreases with increasing spectral separation between modes. T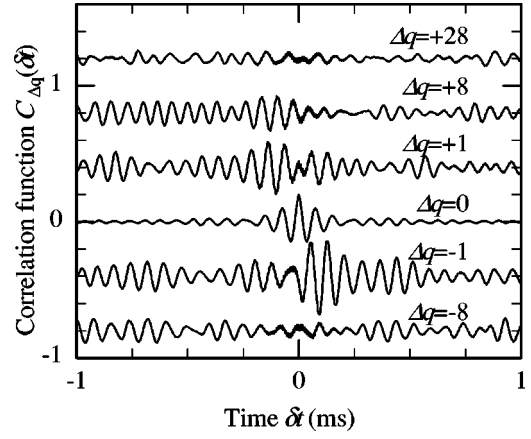he largest correlation is observed in a small group of laser modes with comparable power. This correlation leads to the effective compensation of all low-frequency oscillations in the total laser power, except for the principal in-phase relaxation oscillation common to all modes.

V. ANALYTICAL ESTIMATION OF RELAXATION FREQUENCIES

The frequencies of relaxation oscillations in individual laser modes can be determined analytically [29]. For that purpose we use original rate equations (3.1) and (3.2) with normalized variables, Eqs. (3.15)–(3.19), and neglect spontaneous emission and Langevin forces:

$$\frac{d}{d\tau} m_q(\tau) = G b_q m_q \frac{1}{L} \int_0^L dz \, [n(z)\psi_q(z)] - 1, \quad (5.1)$$

$$\frac{d}{d\tau} n(z,\tau) = \eta - n(z) \left[1 + \sum_q b_q m_q \psi_q(z) \right]. \quad (5.2)$$

Assuming that the steady-state solutions $\bar{m}_q$ and $\bar{n}$ are known, we write linearized rate equations for small deviations $\delta m_q = m_q - \bar{m}_q$ and $\delta n = n - \bar{n}$ from these photon numbers and inversion density, respectively.

$$\frac{d}{d\tau} \delta m_q = G b_q \bar{m}_q \frac{1}{L} \int_0^L dz \, (\delta n \, \psi_q), \quad (5.3)$$

$$\frac{d}{d\tau} \delta n = \eta \frac{\delta n}{\bar{n}} - \bar{n} \sum_p b_p (\delta m_p) \psi_p. \quad (5.4)$$

Substituting $\{\delta m_q, \delta n\}$ by $\{\delta m_q', \delta n'\} \exp(\lambda \tau)$ and inserting in Eqs. (5.3) the solution for δn from Eq. (5.4), we obtain the characteristic equations

$$\lambda \, \delta m_q' + G b_q \bar{m}_q \frac{1}{L} \sum_p b_p(\delta m_p') \int \frac{\bar{n}\psi_q\psi_p}{\lambda + \eta/\bar{n}} dz = 0. \tag{5.5}$$

Assuming that the saturation of the active medium by many longitudinal modes in the laser is uniform ($\bar{n} \cong 1$), that the relative gain rates in all oscillating modes are close to unity ($b_q \cong 1$), and taking into account orthogonality of the modal eigenfunctions ψ_q, we obtain a homogeneous set of algebraic equations for the eigenvalues λ and eigenvectors m_q,

$$\delta m_q' \left[\lambda(\lambda + \eta) + \frac{1}{2} G\bar{m}_q \right] + G\bar{m}_q \sum_p \delta m_p' = 0. \tag{5.6}$$

The eigenvalues are found by equating to zero the determinant of this set of equations:

$$\begin{vmatrix} \lambda(\lambda + \eta) + \dfrac{3}{2} G\bar{m}_{q_{\min}} & G\bar{m}_{q_{\min+1}} & \cdots & G\bar{m}_{q_{\max}} \\[2ex] G\bar{m}_{q_{\min}} & \lambda(\lambda + \eta) + \dfrac{3}{2} G\bar{m}_{q_{\min+1}} & \cdots & G\bar{m}_{q_{\max}} \\[2ex] \cdots & \cdots & \cdots & \cdots \\[2ex] G\bar{m}_{q_{\min}} & G\bar{m}_{q_{\min+1}} & \cdots & \lambda(\lambda + \eta) + \dfrac{3}{2} G\bar{m}_{q_{\max}}, \end{vmatrix} = 0, \tag{5.7}$$

where $q_{\min}$ and $q_{\max}$ are the first and last laser modes at the red and blue side of the emission spectrum ($q_{\max} - q_{\min} = \mathcal{N} - 1$). Equation (5.7) can be modified into

$$\left[1 + \sum_q \frac{G\bar{m}_q}{\lambda(\lambda + \eta) + \dfrac{1}{2} G\bar{m}_q} \right] \prod_q \left[\lambda(\lambda + \eta) + \frac{G\bar{m}_q}{2} \right] = 0. \tag{5.8}$$

Assuming that the power in all laser modes is different, Eq. (5.8) is equivalent to

$$1 + \sum_q \frac{G\bar{m}_q}{\lambda(\lambda + \eta) + \dfrac{1}{2} G\bar{m}_q} = 0. \tag{5.9}$$

The second multiplicative term in Eq. (5.8) gives no additional solutions, since at the points where it approaches zero $[\lambda(\lambda + \eta) + \frac{1}{2} G\bar{m}_q = 0]$, the first term reciprocally approaches infinity.

Analysis of Eq. (5.9) shows that its roots include one large value, λ_0, and $\mathcal{N} - 1$ much smaller values, λ_i, located at

$$\frac{1}{2} G\bar{m}_i < -\lambda_i(\lambda_i + \eta) < \frac{1}{2} G\bar{m}_{i-1}. \tag{5.10}$$

Here the enumeration of the laser modes is taken to extend from the strongest mode with $i=0$ to the weakest mode with $i = \mathcal{N} - 1$. Taking into account that with a large number of oscillating modes $\bar{m}_{i-1} \cong \bar{m}_i$ we estimate the values of the $\mathcal{N} - 1$ smaller eigenvalues to be

$$\lambda_q \cong -\frac{\eta}{2} \pm \sqrt{\left(\frac{\eta}{2}\right)^2 - \frac{G\bar{m}_q}{2}}. \tag{5.11}$$

With most solid-state lasers $G \gg 1$ (e.g., in our experiment $G = 245\,000$), and Eq. (5.11) can be approximated as

$$\lambda_q \cong \pm \sqrt{-\frac{G\bar{m}_q}{2}}. \tag{5.12}$$

Since G and $\bar{m}_q$ are positive numbers, the solutions of Eqs. (5.12) are complex and the photon numbers in the laser modes, $\delta m_q = m_q - \bar{m}_q$, oscillate with frequencies

$$2\pi\nu_q \gtrsim \sqrt{\frac{1}{2} \gamma B_{q_0} M_q}, \tag{5.13}$$

where physical variables are used again instead of normalized variables. This dependence is shown in Fig. 15 by the straight line. It matches very well both the simulated and experimental data points and thus proves the validity of the approximations for the multimode laser described above.

The large eigenvalue λ_0 can be also calculated from Eq. (5.9) assuming in addition that $-\lambda^2 \gg \frac{1}{2} G\bar{m}_q$ as

$$\lambda_0 \cong \sqrt{-G \sum_q \bar{m}_q}. \tag{5.14}$$

Going back to physical variables and taking into account that the stationary solution for the total photon number is $\Sigma_q M_q = (A/B)(\eta - 1)$, we can easily obtain from Eq. (5.14) the well-known solution given by Eq. (2.1). From Eqs. (5.12) and (5.14) one can notice that if the laser has $\mathcal{N}$ effectively oscillating modes of the same amplitude, then

$$\nu_q = \nu_0 \sqrt{\frac{\overline{m_q}}{2 \sum_q \overline{m_q}}} \cong \frac{\nu_0}{\sqrt{2\mathcal{N}}}. \qquad (5.15)$$

This relation agrees well with the experimental data in Fig. 5 with $\nu_0 = 118$ kHz, $\nu_q = 11.8$ kHz, and $\mathcal{N} = 55$ (Fig. 3). The reason for a small deviation of this value from $\mathcal{N} = 50$, calculated with Eq. (5.15), is that the recorded mode was located in the center of the laser emission such that its power was higher than the average. Thus the effective number of oscillating modes at that power is reduced.

VI. SUMMARY

The low-frequency dynamics of multimode class-B lasers has been studied theoretically and experimentally for a Nd^{3+}-doped glass chip laser. This laser oscillates in many longitudinal modes due to a large contribution of inhomogeneous broadening of the gain. In cw operation this laser shows 15% fluctuations of the modal power and 3% fluctuations of the total laser power that are driven by quantum noise. The strength of these fluctuations is determined by mode coupling that emerges here from spatial inhomogeneity.

Power spectra of the modal emission reveal two dominant frequencies of these fluctuations: (i) the highest frequency ν_0, which is common for all modes and corresponds to in-phase oscillations of all laser modes, and (ii) the lower frequency ν_q, which is specific for each mode and corresponds to antiphase oscillations. The frequency of in-phase oscillations depends on the total power of the laser and represents the well-known relaxation oscillations in class-B lasers. The frequency of the antiphase oscillation does not depend on the total power, but only on the modal power. An analytically derived estimate for the frequency of antiphase oscillations accurately reproduces the experimental as well as numerically simulated data, if the number of oscillating modes is large. Similar oscillations appear in polarization laser modes when the output power is recorded behind a polarizer. They are determined by the spatial inhomogeneity of the azimuthal distribution of the laser gain.

Antiphase oscillations in individual modes are compensated by all other modes, such that they disappear in the total laser output. Cross-correlation functions of modal power show that sufficient compensation is ensured by the neighboring modes of about the same power. Therefore, only one frequency peak of the dominant antiphase oscillations is observed in the modal power in a really multimode lasers ($\mathcal{N} \gg 10$). This is in contrast to lasers where only 2 to 8 modes are oscillating, and all relaxation frequencies can show up in each of the laser modes [11,14–17,23,24].

Numerical simulations are based on the Tang, Statz, and deMars rate equations that are extended by mixed-frequency terms, and by Langevin forces simulating quantum noise. Mixed-frequency terms are important for the description of laser dynamics if the inversion density varies along the cavity. This happens, e.g., when the pump light is strongly absorbed by the gain medium and/or if the gain medium does not occupy the total length of the cavity.

The results obtained by numerical simulations show that quantum noise is an important feature, which cannot be neglected in simulating the dynamics of class-B lasers. This alone results in the observed strong fluctuations of the modal and total output. This feature will be especially important for the preparation of stable laser light sources, and for sensitive absorption measurements in the laser cavity.

[1] V. M. Baev, T. Latz, and P. E. Toschek, Appl. Phys. B: Lasers Opt. **69**, 171 (1999).

[2] A. V. Ghiner, K. P. Komarov, and K. G. Folin, Opt. Commun. **19**, 350 (1975).

[3] S. A. Kovalenko, Kvant. Elektron. **8**, 1271 (1981) [Sov. J. Quantum Electron. **11**, 759 (1981)].

[4] V. M. Baev, G. Gaida, H. Schröder, and P. E. Toschek, Opt. Commun. **38**, 309 (1981).

[5] Yu. M. Aivazyan, V. M. Baev, V. V. Ivanov, S. A. Kovalenko, and E. A. Sviridenkov, Kvant. Elektron. **14**, 279 (1987) [Sov. J. Quantum Electron. **17**, 168 (1987)].

[6] I. McMackin, C. Radzewicz, M. Beck, and M. G. Raymer, Phys. Rev. A **38**, 820 (1988).

[7] J. Sierks, T. Latz, V. M. Baev, and P. E. Toschek, Phys. Rev. A **57**, 2186 (1998).

[8] Yu. M. Aivazjan, V. V. Ivanov, S. A. Kovalenko, V. M. Baev, E. A. Sviridenkov, H. Atmanspatcher, and H. Scheingraber, Appl. Phys. B: Photophys. Laser Chem. **2**, 175 (1988).

[9] Yu. M. Aivazjan, V. M. Baev, A. A. Kachanov, and S. A. Kovalenko, Kvant. Elektron. **13** 1723 (1986) [Sov. J. Quantum Electron. **16**, 1133 (1986)].

[10] T. Baer, J. Opt. Soc. Am. B **3**, 1175 (1986).

[11] K. Otsuka, P. Mandel, and E. A. Viktorov, Phys. Rev. A **56**, 3226 (1997).

[12] C. J. Kennedy and J. D. Barry, IEEE J. Quantum Electron. **QE-10**, 595 (1974).

[13] G. E. James, E. M. Harrel II, C. Bracikowski, K. Wiesenfeld, and R. Roy, Opt. Lett. **15**, 1141 (1990).

[14] K. Otsuka, P. Mandel, S. Bielawski, D. Derozier, and P. Glorieux, Phys. Rev. A **46**, 1692 (1992).

[15] P. Mandel, M. Georgiou, K. Otsuka, and D. Pieroux, Opt. Commun. **106**, 341 (1993).

[16] E. Lacot and F. Stoeckel, J. Opt. Soc. Am. B **13**, 2034 (1996).

[17] P. Mandel, B. A. Nguyen, and K. Otsuka, Quantum Semiclassic. Opt. **9**, 365 (1997).

[18] C. L. Tang, H. Statz, and G. de Mars, J. Appl. Phys. **34**, 2289

(1963).

[19] D. Pieroux and P. Mandel, Quantum Semiclassic. Opt. **9**, L17 (1997).

[20] P. A. Khandokhin, Ya. I. Khanin, Yu. Mamaev, N. Milovski, E. Shirokov, S. Bielawski, D. Derozier, and P. Glorieux, Kvant. Elektron. **25**, 517 (1998) [Sov. J. Quantum Electron. **28**, 502 (1998)].

[21] K. Wiessenfeld, C. Bracikowski, G. James, and R. Roy, Phys. Rev. Lett. **65**, 1749 (1990).

[22] P. Khandokhin, Ya. Khanin, J.-C. Celet, D. Dangoisse, and P. Glorieux, Opt. Commun. **123**, 372 (1996).

[23] L. Stamatescu and M. W. Hamilton, Phys. Rev. E **55**, 2115 (1997).

[24] N. B. Abraham, L. Sekaric, L. L. Carson, V. Seccareccia, P. A. Khandokhin, Ya. I. Khanin, I. V. Koryukin, and V. G. Zhislina, Phys. Rev. A **62**, 013810 (2000).

[25] M. Lax, in *Statistical Physics. Phase Transitions and Superfluidity*, edited by M. Chretien, E. P. Gross, and S. Deser (Gordon

& Breach, New York, 1968), pp. 277–475.

[26] P. A. Khandokhin, P. Mandel, I. V. Koryukin, B. A. Nguyen, and Ya. I. Khanin, Phys. Lett. A **235**, 248 (1997).

[27] V. Magni, G. Gerullo, S. De Silvestri, O. Svelto, L. J. Qian, and M. Danailov, Opt. Lett. **18**, 2111 (1993).

[28] A. S. Meller, P. A. Khandokhin, and Ya. I. Khanin, Kvant. Elektron. **13**, 2278 (1986) [Sov. J. Quantum Electron. **16**, 1502 (1986)].

[29] Ya. I. Khanin, *Principles of Laser Dynamics* (North-Holland, Amsterdam, 1995).

[30] W. H. Keen and J. A. Weiss, Appl. Opt. **3**, 545 (1963).

[31] J. Hünkemeier, R. Böhm, V. M. Baev, and P. E. Toschek, Opt. Commun. **176**, 417 (2000).

[32] A. E. Siegman, *Lasers* (University Science Books, Mill Valley, CA, 1986), p. 963.

[33] P. A. Khandokhin, E. A. Ovchinnikov, and E. Yu. Shirokov, Phys. Rev. A **61**, 053807 (2000).